

Ultra-Broadband Super-Planckian Radiative Heat Transfer with Artificial Continuum Cavity States in Patterned Hyperbolic Metamaterial

Jin Dai,¹ Fei Ding,² Sergey I. Bozhevolnyi,² and Min Yan¹

¹*Department of Applied Physics, School of Engineering Sciences,
KTH-Royal Institute of Technology,
Electrum 229, 16440 Kista, Sweden**

²*Centre for Nano Optics, University of Southern Denmark,
Campusvej 55, DK-5230 Odense, Denmark*

(Dated: June 13, 2021)

Abstract

Localized cavity resonances due to nanostructures at material surfaces can greatly enhance radiative heat transfer (RHT) between two closely placed bodies owing to stretching of cavity states in momentum space beyond light line. Based on such understanding, we numerically demonstrate the possibility of ultra-broadband super-Planckian RHT between two plates patterned with trapezoidal-shaped hyperbolic metamaterial (HMM) arrays. The phenomenon is rooted not only in HMM's high effective index for creating sub-wavelength resonators, but also its extremely anisotropic isofrequency contour. The two properties enable one to create photonic bands with a high spectral density to populate a desired thermal radiation window. At sub-micron gap sizes between such two plates, the artificial continuum states extend outside light cone, tremendously increasing overall RHT. Our study reveals that structured HMM offers unprecedented potential in achieving a controllable super-Planckian radiative heat transfer for thermal management at nanoscale.

PACS numbers: 44.40.+a, 73.20.Mf

Near-field-mediated radiative heat transfer (RHT) exceeding the far-field blackbody limit [1] has attracted increased attention in recent years [2], not only because it unfolds an un-explored fundamental scientific field, but also because it holds technological importance towards nano-gap thermophotovoltaics, scanning near-field thermal microscopy, thermal logics etc. Commonly, materials supporting surface-guided waves at infrared frequency were investigated for achieving such phenomenon, since surface modes especially at frequency close to their resonances offer extra channels of energy transfer due to evanescent-wave coupling at small gaps. Surface-wave-bearing materials at infrared include polar dielectrics supporting surface phonon polaritons [3, 4], doped silicon supporting surface plasmon polaritons [5], and more recently grooved metal surfaces supporting the so-called spoof surface plasmon polaritons [6–9]. The presence of surface modes leads to spectrally enhanced quasi-monochromatic heat flux around their resonance frequencies. Contrary to the extensive attentions paid to surface modes, *localized resonant modes* were rarely mentioned for achieving near-field-enhanced RHT. Localized or cavity resonances at infrared or even optical frequencies can be readily created using today’s nanofabrication technologies. Spatial localization of such modes usually corresponds to enormous extension of the modes in momentum (wave vector \mathbf{k}) dimension. Such flat bands can potentially lie outside light cone (bounded by $k = \omega/c$) in frequency-momentum representation. Similar to surface-mode-based RHT scenario, presence of photonic states outside light cone implies near-field energy transfer between two bodies, which can potentially amount to super-Planckian RHT. A direct advantage of cavity-resonance-based RHT is that one can arrange nano-cavities with different resonant frequencies within unit cells of two plates to achieve enhanced RHT at multiple frequencies. With an exotic resonator design, as the current work will reveal, an ultra-broadband super-Planckian RHT can even be achieved.

Referring to Fig. 1, we consider RHT between two plates each consisting a gold substrate and an array of trapezoidal-shaped hyperbolic metamaterial (HMM). The HMM is formed by a multi-layer metal-dielectric stack. The two plates are separated by a vacuum gap g . The thicknesses of dielectric and metal are 95 and 20 nm, respectively. Each HMM cavity contains 20 dielectric-metal pairs. The cross-section of a single cavity resembles a trapezoid with short base of $w_t = 0.4 \mu\text{m}$, long base of $w_b = 1.9 \mu\text{m}$, and height of $h = 2.3 \mu\text{m}$. The period of the HMM arrays is fixed at $a = 2.0 \mu\text{m}$. The relative permittivities of dielectric (Si) and metal (Au) are $\epsilon_{\text{Si}} = 11.7$ and $\epsilon_{\text{Au}}(\omega) = 1 - \frac{\omega_p^2}{\omega(\omega+i\gamma)}$, in which $\omega_p = 9 \text{ eV}$,

and $\gamma = 35$ meV, respectively. Such structure can be fabricated with focused ion beam milling of deposited metal-dielectric multilayers [10], or with shadow deposition of dielectric and metal layers [11, 12].

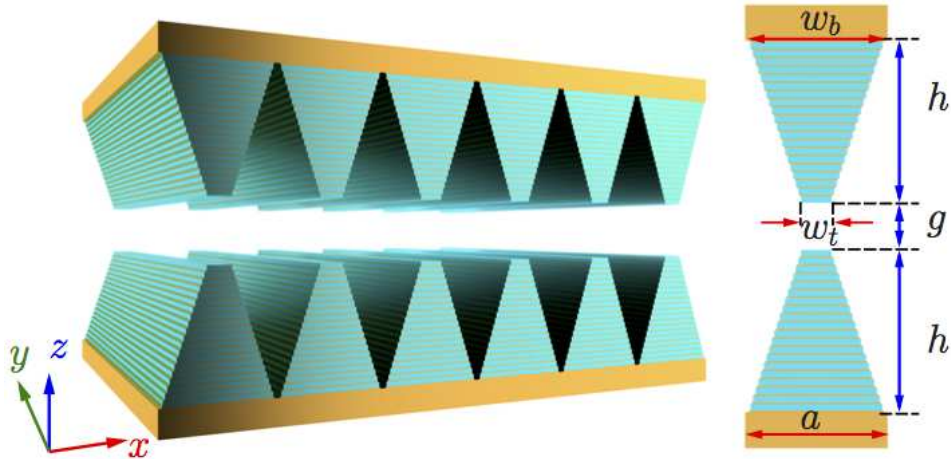


FIG. 1. (Color online). Schematic of the trapezoidal-shaped HMM plates. The cyan and orange layers denote dielectric and gold layers, respectively.

The HMM, when truncated, helps to create *subwavelength* electromagnetic cavities, while the trapezoidal geometry is responsible for producing such resonances over a broad wavelength range. To simplify our argument in this paragraph, we neglect the gold substrates[13] and consider only k_x wave-vector direction. A single HMM plate, when un-patterned, has an *indefinite* diagonal effective permittivity tensor, with negative x and y components and positive z component. Such an anisotropic slab, for the given geometry, guides a set of x -propagating p -polarized modes [14]. For frequency up to 300×10^{12} rad/s and even higher, the modes have *almost similar* linear dispersion curves, based on which one calculates the effective index (n_{eff}) of the HMM as ~ 3.77 . When laterally truncated, p -polarized wave bounces between two truncation facets; each HMM patch therefore is a 2D *high-index* resonator. High-index material is essential for creating small-dimension resonators, especially at the upper wavelength limit for broadband RHT, that fit into a grating period a . Note also that, for achieving super-Planckian RHT at a wavelength λ_r , a needs to satisfy $a < \lambda_r/2$ in order for the resonance to cross light line in the first Brillouin zone of the plate's mode spectrum. The lower wavelength limit λ_{min} of desired broadband RHT would set $a < \lambda_{\text{min}}/2$. The most intriguing property of such a HMM resonator, as will be further clarified in Fig. 3,

is the weak dependence of its resonant frequencies on mode orders (with nodal breaking along z), or equivalently the resonator's thickness. This sets the fundamental difference between using HMM and using an isotropic dielectric material. A trapezoidal profile-patterned HMM can therefore be treated as a series of vertically-stacked thin HMM resonators of varying widths, and in turn varying resonant frequencies, for achieving broadband operation.

We mention that a single array of such HMM resonators was previously found to exhibit broadband absorption of far-field radiation [15]. Near-field properties with implications to RHT were insofar left unexplored. There were also studies of RHT based on un-patterned HMM plates [16–21]; the results, as we will show later, can be radically different from RHT between patterned HMMs, principally due to lack of localized resonances. Here, using a rigorous full-wave scattering-matrix method [6, 9], we calculate the RHT flux between two patterned HMM plates and numerically confirm ultra-broadband super-Planckian RHT at small gap sizes. In addition, we utilize a finite-element based eigen-mode solver [22, 23] to reveal the modal properties of the double-plate structure and identify that cavity modes play critical roles in enhancing RHT.

The radiative heat flux between two 1D periodic arrays can be expressed by

$$q(T_1, T_2) = \frac{1}{2\pi} \int_0^\infty [\Theta(\omega, T_1) - \Theta(\omega, T_2)] \Phi(\omega) d\omega, \quad (1)$$

where $\Theta(\omega, T) = \hbar\omega / \exp[(\hbar\omega/k_B T) - 1]$ is the mean energy of Planck oscillators at temperature T and angular frequency ω . Φ is integrated transmission factor

$$\Phi(\omega) = \frac{1}{4\pi^2} \sum_{j=s,p} \int_{-\infty}^{+\infty} \int_{-\frac{\pi}{a}}^{+\frac{\pi}{a}} \mathcal{T}_j(\omega, k_x, k_y) dk_x dk_y. \quad (2)$$

$\mathcal{T}_j(\omega, k_x, k_y)$ is the transmission factor that describes the probability of a thermally excited photon transferring from one plate to the other, given polarization s or p , and surface-parallel wavevector $\mathbf{k}_{\parallel} \equiv (k_x, k_y)$ at ω .

Figure 2 plots the transmission-factor distributions (\mathcal{T} maps) over frequency and k_x , while k_y is kept zero, for three types of plate configurations: unpatterned HMM plates [panels 2(a) and (b)], rectangular-profiled HMM plates [2(d) and (e)], and trapezoidal-profiled HMM plates [2(g) and (h)]. All configurations are mirror-symmetric. Note the \mathcal{T} maps are shown only for k_x direction, along which the mode spectra of truncated HMM structures exhibit marked difference against un-truncated scenario. The calculation is repeated for two gap sizes: 1000 and 50 nm. For comparison purpose, in some \mathcal{T} maps we selectively superimpose

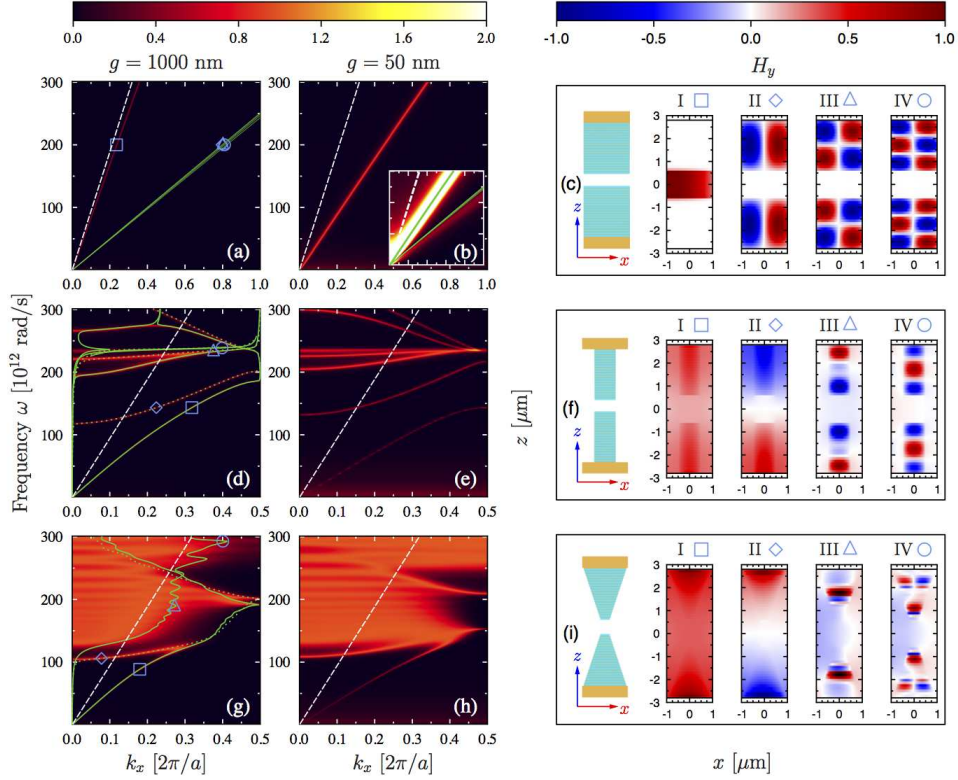


FIG. 2. (Color online). (a,d,g) Transmission-factor maps $\mathcal{T}_{s+p}(\omega, k_x, k_y = 0)$ between two plates with gap $g = 1000$ nm for three configurations: (a) unpatterned HMM plates; (d) rectangular-profiled HMM plates $w_t = w_b = 1000$ nm; (g) trapezoidal-profiled HMM plates. (b,e,h) The same but for $g = 50$ nm. The inset in (b) has a down-limited color scale (0, 0.01). Dashed white line indicates light line in vacuum. Green lines are guided modes by the two-plate structure obtained through eigen-mode analysis, solid lines for bonding modes and dotted lines for anti-bonding modes. (c,f,g) Schematic structure units, as well as representative mode fields marked in (a,d,g).

dispersion curves obtained from eigen-mode calculations. In Fig. 2(a), when HMM is untruncated ($g = 1000$ nm), the \mathcal{T} map shows a thin line of states just below light line. The states originate from a gap plasmon mode (GPM) confined mostly in the vacuum gap between the two HMM plates, as confirmed by the mode distribution [mode I in panel (c), or c-I] from eigen-mode analysis. Further below the GPM states, there are a set of modes (c-II, c-III, c-IV) guided mostly in the HMMs; the number of modes is decided by the number of metal-dielectric layer pairs constructing the HMMs [14]. Only the bonding-type HMM-guided modes are shown. Owing to their strong confinements and the relatively

large gap size, the fields in two HMM plates are hardly coupled, therefore having almost no contribution to the RHT process. Even when separation between the two plates is reduced to $g = 50\text{nm}$, the contribution of the HMM-guided modes to RHT is trivial, as shown by the \mathcal{T} map in Fig. 2(b), as well as its inset with a down-limited color scale. When HMM is truncated, mode structure in the two-plate system changes drastically. The GPM remains (f-I), but now with its field confined between the two gold substrates; an anti-bonding GPM (f-II) also emerge due to relatively large separation between two gold plates. Then, importantly, each HMM patch becomes a cavity; localized resonances happen (modes f-III, f-IV). The cavity mode fields are tightly confined laterally, which leads to almost flat dispersion curves of the modes, as shown in Fig. 2(d). The contribution of these cavity modes to RHT is evident in Fig. 2(d) with $g = 1000\text{ nm}$, and even more so in Fig. 2(e) with $g = 50\text{ nm}$.

Unlike resonators made of isotropic dielectric materials, the resonant frequencies of the HMM modes with different order numbers due to nodal breaking along z are quite close to each other. This can be understood by examining the iso-frequency contours of the HMM in bulk, shown in k_x and k_z axes ($k_y = 0$) in Fig. 3. Three hyperbolic contours correspond to relatively close frequencies at $235, 245, \text{ and } 255 \times 10^{12}\text{ rad/s}$. Given a 2D rectangular HMM cavity (of width w) in Fig. 2(f), resonant frequencies of modes are decided by the modes' corresponding k_x and k_z values. The fundamental mode has approximately $k_x = \pi/w$ and $k_z = 1.5\pi/h$ [24]. For next higher-order mode with a nodal breaking along z , k_x remains the same, and it has $k_z = 2.5\pi/h$, and so on. The first three cavity modes are indicated by three yellow dots in Fig. 3, vertically aligned. They are positioned quite near to $245 \times 10^{12}\text{ rad/s}$, which is in reasonably good agreement with Figs. 2(d) and (e). The fact that the modes with nodal breaking along z stay close in frequency is fundamentally decided by the extremely anisotropic hyperbolic iso-frequency curves of the HMM. This is confirmed by a re-plot of Fig. 3 in its inset using equal axis scales. The hyperbolic curves are almost vertically lines.

The iso-frequency plot in Fig. 3 also suggests that it is the width of a 2D HMM cavity which determines the resonant frequencies of its modes. The cavity height (even very thin) does not influence much the resonant frequencies. Knowing this, one can potentially create a cavity that supports resonances at multiple frequencies. Trapezoidal-profiled HMM structure as illustrated in Fig. 1 is a straightforward solution. Indeed, the computed \mathcal{T} map for $g = 1000\text{ nm}$ exhibits ultra-broadband transmission factors [Fig. 2(g)]. The states

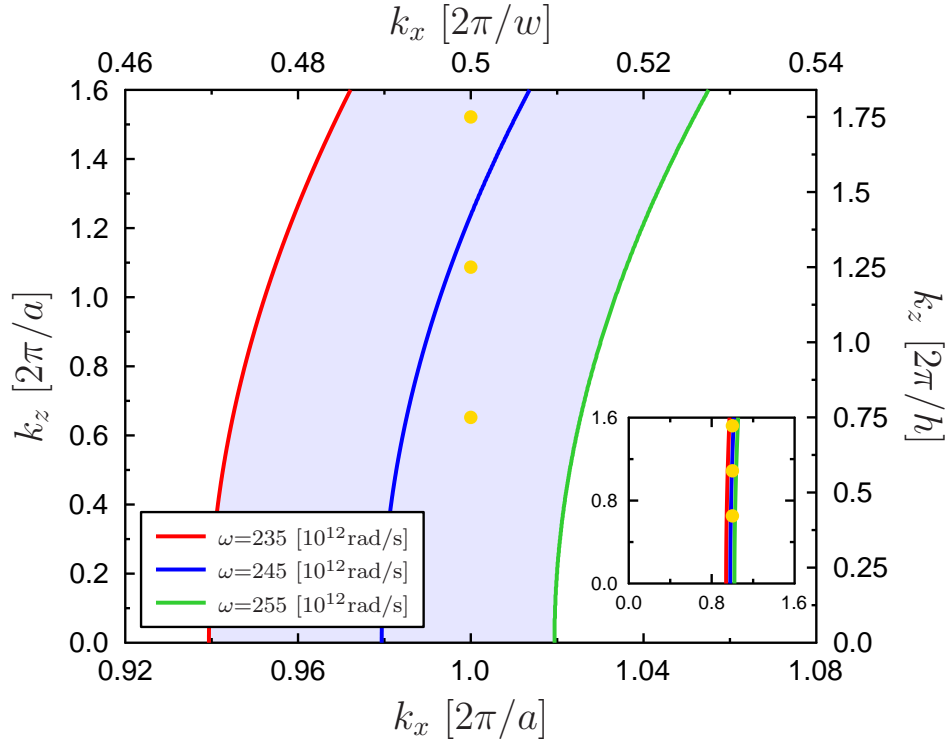


FIG. 3. (Color online). Iso-frequency contours of the bulk HMM at frequencies at 235, 245, and 255×10^{12} rad/s. The yellow dots, from bottom to top, indicate the first three resonant modes of a rectangular HMM cavity as in Fig. 2(f). Inset shows the same plot with equal axis scales.

contributing to RHT are so densely packed such that they form almost a continuum. The lower cut-off frequency of the continuum is determined by the bottom width of the trapezoids. High transmission factors extend beyond light line, and at certain frequencies reach the first Brillouin zone edge. When the gap becomes smaller, at $g = 50$ nm, the continuum states extend to larger k_x values; more evanescent states contribute to RHT. This lends the possibility of achieving an ultra-broadband super-Planckian RHT between two plates using trapezoidal-profiled HMMs. From eigen-mode calculations, we obtain modes responsible for the RHT process. Besides the GPM pair (modes i-I, i-II), we show modes i-III and i-IV, which offer a glimpse of cavity modes in the continuum. As characterized by their hot spots, the cavity modes now have very tight z confinement, or correspondingly large k_z . The positions of hot spots reveal the mechanisms of their resonances. Mode i-III has hot spots at the middle section of the trapezoidal HMM cavity; it well corresponds to a resonant frequency just below 200×10^{12} rad/s. Slight complication arises at higher frequencies. Mode i-IV,

for example, has its hot spots located at both narrow- and wide-width sections of the HMM cavity; a wide HMM section can support a high-frequency resonance through nodal breaking along x direction.

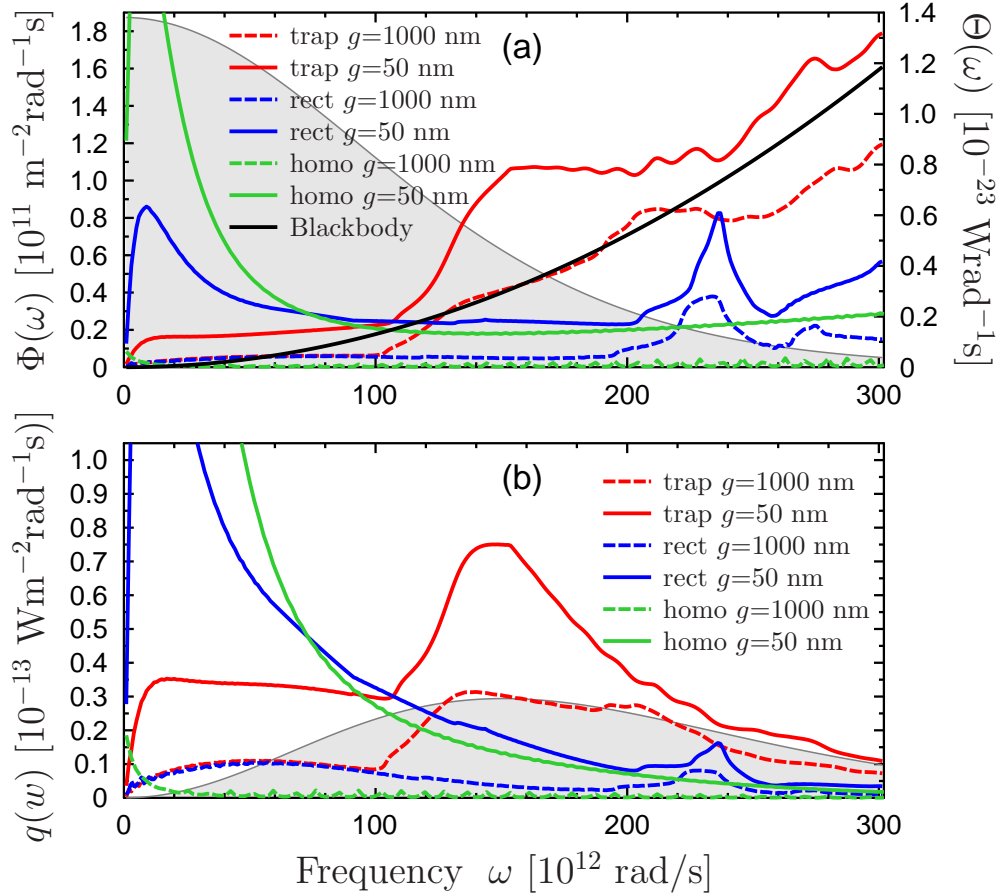


FIG. 4. (Color online). (a) Integrated transmission-factor spectra $\Phi(\omega)$ for three types of two-plate structures: trapezoidal-profiled (trap) HMM plates, rectangular-profiled (rect) HMM plates, and homogeneous (homo) HMM plates. Results for two gap sizes 1000 and 50 nm are presented. Black line represents integrated Φ spectrum between two blackbodies. (b) Spectral heat flux $q(\omega)$ for the same configurations as in (a) for plate temperatures at 301 and 300 K. The thin gray lines with shading in (a) and (b) indicate Planck's oscillator term $\Theta(\omega, 301 \text{ K}) - \Theta(\omega, 300 \text{ K})$ and spectral heat flux between two blackbodies, respectively.

A full characterization of RHT between two plates requires a calculation of transmission factors for all \mathbf{k}_{\parallel} over concerned frequency range. In Supplemental Material, we selectively plot $\mathcal{T}_{s+p}(k_x, k_y)$ maps at $\omega = 173 \times 10^{12}$ rad/s for various gap sizes. There we also explain the

modal origin of the RHT states with the help of eigen-mode analysis especially when $k_x = 0$ and $k_y \neq 0$. Generally speaking, as \mathbf{k}_{\parallel} deviates from x direction, the near-field contribution to RHT becomes less significant, but the far-field contribution persists. The decreasing near-field contribution is expected since each HMM patch no longer sustains cavity resonances when \mathbf{k}_{\parallel} deviates from x direction. The volumetric transmission-factor data were integrated with respect to \mathbf{k}_x and \mathbf{k}_y . In Fig. 4(a) we plot the integrated transmission-factor spectra, $\Phi(\omega)$, for the three types of HMM plate configurations as mentioned in Fig. 3 at gap sizes of 1000 and 50 nm. The trapezoidal-profiled HMM plates clearly exhibit the highest Φ over almost the whole frequency range when $g = 1000$ nm; at $g = 50$ nm, it has the highest Φ among the three structures at high frequencies (above $\sim 110 \times 10^{12}$ rad/s). At low frequencies, the homogeneous HMM plates have better RHT performance at small gap sizes. That is because the effect of eddy current generation through magnetic-field coupling (s polarization) between metal plates becomes prominent [9, 25]; and the surface area at the nearest proximity between two plates decides the degree of such coupling (*i.e.* Derjaguin proximity approximation starts to apply). The broadband high Φ for the trapezoidal-is dominantly due to the cavity mode continuum as shown in Figs. 3(g) and (h). The rectangular-profiled HMM plates show high Φ bands at certain frequencies (mainly at $\sim 235 \times 10^{12}$ rad/s) linked to cavity resonances in the HMM patches, as indicated in Fig. 3(d) and (e). It is worth noticing that the peak Φ value of the rectangular-profiled HMM structure is smaller than that of the trapezoidal-profiled HMM structure at the same frequency. This is due to the fact that the trapezoidal one can have extra resonances due to nodal breaking in x direction, while similar high-order resonances do not exist for the rectangular counterpart in the considered frequency range. The homogeneous HMM structure shows featureless Φ spectra, because they do not sustain any cavity resonances but linearly dispersive guided modes [Fig. 3(a) and (b)]. As the gap size decreases down to 50 nm, the Φ spectrum of the trapezoidal-profiled HMM structure surpasses that of blackbody structure over the whole frequency range; ultra-broadband super-Planckian RHT occurs. We further calculate spectral heat flux $q(\omega)$ between two plates with temperatures at 301 and 300 K for the mentioned HMM structures [Fig. 4(b)]. At $g = 50$ nm, the trapezoidal structure performs significantly better than blackbody plates, with 155% increase in q at the highest- q frequency of the blackbody-plate scenario (*i.e.*, 150×10^{12} rad/s). Note that the structure presented in this work is for demonstrating the flexibility of HMM-based plates for tailoring enhanced

near-field RHT [Φ spectra in Fig. 4(a)] without considering specific plate temperatures in the first place. The actual heat transfer in measurable values [as q spectra in Fig. 4(b)] depends further on exact temperature settings. In reality, towards a particular application, one should design the profile patterning (period, resonator width, trapezoid shape, etc) such that one maximize near-field RHT in measurable quantities either at a desired frequency range or over the whole spectrum.

The profile-patterning of HMM layers is currently one dimensional, which results in inferior RHT when \mathbf{k}_{\parallel} has inclination towards y direction. We envisage that a 2D periodic structuring of the HMM layer (pyramid array) [10] can give rise to isotropic enhancement in RHT in all \mathbf{k}_{\parallel} directions owing to true localization of the cavities modes. In addition, in this work we have not optimized the metal and dielectric layer thicknesses (as well as the dielectric material type) in the HMM. It is likely one can have even higher effective index of the HMM by choosing appropriate geometrical and material parameters, so that one can further adjust the frequency range of the cavity mode continuum as well as the Brillouin zone size.

In conclusion, we numerically demonstrated one can achieve an ultra-broadband super-Planckian RHT with two closely spaced trapezoidal-profiled HMM plates. The design rests on two key properties of HMMs: high effective index for creating sub-wavelength resonators, and extremely anisotropic iso-frequency curves responsible for cavity-width-dependent resonance frequencies. The superiority of the trapezoidal-profiled patterning in achieving ultra-broadband enhanced RHT is explained through its capability of forming a cavity mode continuum. The transmission-factor maps derived from scattering-matrix method were confirmed by dispersion curves calculated using an eigen-mode mode solver. The contributing modes were further elucidated with the obtained mode field distributions. Our study reveals that highly localized cavity resonances, besides surface waves, do enhance RHT at small separation of two bodies. In this respect, structured hyperbolic media offers unprecedented control in creating cavity modes for achieving a controllable super-Planckian RHT.

J. D. and M. Y. acknowledge support by the Swedish Research Council (VR) via project 2011-4526, and VR's Linnaeus center in Advanced Optics and Photonics. F. D. and S. I. B. acknowledge support from the Danish Council for Independent Research via project 1335-00104. The simulations were performed on the Swedish National Infrastructure for Computing (SNIC).

* e-mail: jind@kth.se

- [1] D. Polder and M. van Hove, *Phys. Rev. B* **4**, 3303 (1971).
- [2] A. I. Volokitin and B. N. J. Persson, *Rev. Mod. Phys.* **79**, 1291 (2007).
- [3] M. F. Vaillon, M. P. Mengüç, and Rodolphe, *J. Phys. D: Appl. Phys.* **43**, 75501 (2010).
- [4] S. A. Dyakov, J. Dai, M. Yan, and M. Qiu, *Phys. Rev. B* **90**, 045414 (2014).
- [5] E. Rousseau, M. Laroche, and J.-J. Greffet, *Appl. Phys. Lett.* **95** (2009).
- [6] R. Guérout, J. Lussange, F. S. S. Rosa, J.-P. Hugonin, D. A. R. Dalvit, J.-J. Greffet, A. Lambrecht, and S. Reynaud, *Phys. Rev. B* **85**, 180301 (2012).
- [7] J. Dai, S. A. Dyakov, and M. Yan, *Phys. Rev. B* **92**, 035419 (2015).
- [8] J. Dai, S. A. Dyakov, and M. Yan, *Phys. Rev. B* **93**, 155403 (2016).
- [9] J. Dai, S. A. Dyakov, S. I. Bozhevolnyi, and M. Yan, *Phys. Rev. B* **94**, 125431 (2016).
- [10] F. Ding, Y. Jin, B. Li, H. Cheng, L. Mo, and S. He, *Laser Photon. Rev.* **8**, 946 (2014).
- [11] X. Yang, J. Yao, J. Rho, X. Yin, and X. Zhang, *Nat. Photon.* **6**, 450 (2012).
- [12] J. Zhou, A. F. Kaplan, L. Chen, and L. J. Guo, *ACS Photonics* **1**, 618 (2014).
- [13] The gold substrates are mainly to prevent transmission leakage; their presence also induces a surface mode between HMM and gold. However, the main contribution to near-field RHT is the cavity modes, whose existence persist even without the gold substrates.
- [14] M. Yan, L. Thylén, and M. Qiu, *Opt. Express* **19**, 3818 (2011).
- [15] Y. Cui, K. H. Fung, J. Xu, H. Ma, Y. Jin, S. He, and N. X. Fang, *Nano Letters* **12**, 1443 (2012).
- [16] S.-A. Biehs, M. Tschikin, R. Messina, and P. Ben-Abdallah, *Appl. Phys. Lett.* **102**, 131106 (2013).
- [17] Y. Guo and Z. Jacob, *Opt. Express* **21**, 15014 (2013).
- [18] Y. Guo, C. L. Cortes, S. Molesky, and Z. Jacob, *Appl. Phys. Lett.* **101**, 131106 (2012).
- [19] O. D. Miller, S. G. Johnson, and A. W. Rodriguez, *Phys. Rev. Lett.* **112**, 157402 (2014).
- [20] S.-A. Biehs, M. Tschikin, and P. Ben-Abdallah, *Phys. Rev. Lett.* **109**, 104301 (2012).
- [21] X. Liu and Z. Zhang, *ACS Photonics* **2**, 1320 (2015).
- [22] G. Parisi, P. Zilio, and F. Romanato, *Opt. Express* **20**, 16690 (2012).
- [23] C. Fietz, Y. Urzhumov, and G. Shvets, *Opt. Express* **19**, 19027 (2011).

- [24] Extra 0.5π phase change is due to nearly perfect magnetic conductor condition at boundary in contact with gold.
- [25] P.-O. Chapuis, S. Volz, C. Henkel, K. Joulain, and J.-J. Greffet, Phys. Rev. B **77**, 035431 (2008).

Supplemental Material

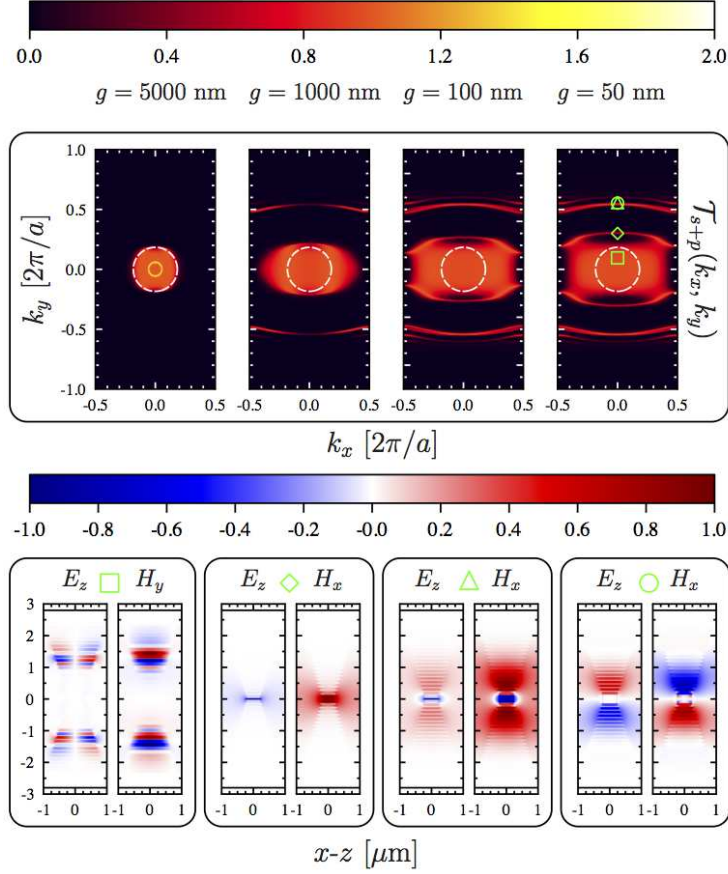


FIG. 5. (Color online). Upper panels show transmission factor maps $\mathcal{T}_{s+p}(k_x, k_y)$ between the two trapezoidal-profiled HMM plates at four gap sizes at $\omega = 173 \times 10^{12}$ rad/s. Both polarizations are included. Circles in dashed white lines are light cones. Lower panels present four modes in their respective major electric- and magnetic-field components at various k_y values ($k_x = 0$) for the structure with $g = 50$ nm.

Figure 5 shows transmission-factor (\mathcal{T}) maps as a function of surface-parallel wavevectors (k_x, k_y) at a fixed frequency $\omega = 173 \times 10^{12}$ rad/s for the trapezoidal-profiled HMM plate structure discussed in the main text. Four scenarios corresponding to gap sizes of 5000, 1000, 100, and 50 nm are shown. Integration of each spectra over k_x and k_y gives rise to the integrated transmission-factor Φ at this frequency.

From the upper panels in Fig. 5, one sees that at larger gap sizes the contribution to radiative heat transfer (RHT) mainly comes from electromagnetic states inside light cone.

These states correspond to thermally excited photons radiating away from one plate to the other. It is interesting to notice that the combined $s + p$ states are almost isotropic in the (k_x, k_y) plane; they form nearly unitary transmission factors filling the whole light cone. The amplitude of the transmission factors are still less than those between two ideal blackbody plates, which would have a uniform amplitude of two filling the whole light cone. As the gap size decreases, states outside the light cone come into play, suggesting more and more near-field contributions to RHT. At $g = 1000$ nm, the integrated transmission factor at this frequency is already beyond that between the far-field blackbody limit [see Fig. 4(a) in the main article].

Besides the main block of RHT states connected to light cone, there are discrete thin lines of states emerging and their contributions become more significant as gap size decreases. To better understand these RHT channels, in the lower panels in Fig. 5 we plot four representative mode fields as marked on the \mathcal{T} spectrum for the $g = 50$ nm configuration. The modes were calculated using a finite-element based eigen-mode solver. We examine particularly modes with $(k_x = 0, k_y \neq 0)$. Mode patterns for $(k_x \neq 0, k_y = 0)$ were presented in Fig. 2 in the main text. The modes in Fig. 5 are nothing but guided modes by the trapezoidal-profiled HMM plates along y direction. Each trapezoidal HMM stack, being structurally invariant in y direction, functions like an electromagnetic waveguide; a single grating with periodic arrangement of such HMM stacks is a waveguide array. Due to high contrast in permittivity values between HMM and vacuum, the guided modes are hybrid in polarization. the mode inside the light cone (marked by green square) is a radiation mode, which is manifested by its rapid variation in mode profile plotted in Fig. 5. The modes outside light cone are in principle similar to those presented for the un-patterned HMM plate structure in Fig. 2(c) in the main article. The mode marked by the diamond is a gap plasmon mode mainly confined inside the air gap between the two HMM stacks. The modes marked by the triangle and the circle are a bonding- and anti-bonding mode pair whose fields are mainly confined in HMMs. Note that, these two HMM-guided modes are the first two (fundamental mode pair), among a set of such HMM-guided modes supported by the system.